ACS APPLIED MATERIALS & INTERFACES

Research Article

www.acsami.org

MoO_2-Ordered Mesoporous Carbon Nanocomposite as an Anode Material for Lithium-Ion Batteries

Lingxing Zeng, Cheng Zheng, Cuilin Deng, Xiaokun Ding, and Mingdeng Wei*

Institute of Advanced Energy Materials, Fuzhou University, Fuzhou, Fujian 350002, China

ABSTRACT: In the present work, the nanocomposite of MoO_2-ordered mesoporous carbon (MoO_2−OMC) was synthesized for the first time using a carbon thermal reduction route and the mesoporous carbon as the nanoreactor. The synthesized nanocomposite was characterized by X-ray diffraction (XRD), thermogravimetric analysis (TGA), N_2 adsorption−desorption, scanning electron microscopy (SEM), and transmission electron microscopy (TEM) measurements. Furthermore, this nanocomposite was used as an anode material for Li-ion intercalation and exhibited large reversible capacity, high rate performance, and good cycling stability. For instance, a high reversible capacity of 689 mAh g^{-1} can remain after 50 cycles at a current density of 50 mA g^{-1}. It is worth mentioning that the MoO_2−OMC nanocomposite electrode can attain a high reversible capacity of 401 mAh g^{-1} at a current density as high as 2 A g^{-1}. These results might be due to the intrinsic characteristics of nanocomposite, which offered a better accommodation of the strain and volume changes and a shorter path for Li-ion and electron transport, leading to the improved capacity and enhanced rate capability.

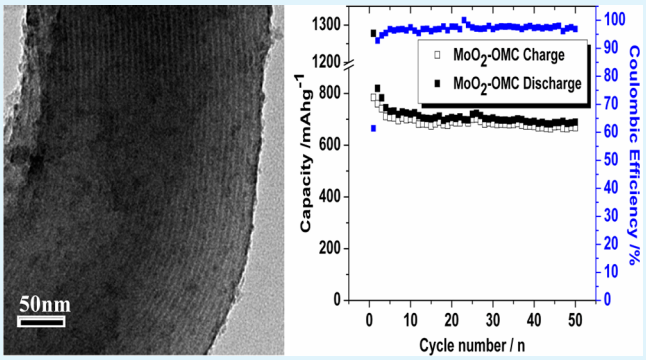

KEYWORDS: *MoO_2−OMC, carbon thermal reduction, anode, lithium-ion batteries*

INTRODUCTION

Nowadays, development of lithium-ion batteries (LIBs) with high power and energy densities for applications in the electric vehicles (EV) and hybrid electric vehicles (HEV) has attracted much attention. However, the performance of LIBs cannot meet the requirements of EV or HEV in terms of high power density, high rate performance, and safety concern.[1,2] The low theoretical capacity of commercial graphite anode (372 $mAhg^{-1}$), large irreversible capacity, and low intercalating potential make it important to find an alternative negative electrode. Thus, the development of new anode materials with a large capacity and high energy density is still a challenge.[3−6]

Molybdenum oxides (MoO_2 and MoO_3) have received much attention due to their low electrical resistivity, high electrochemical activity, and large capacity (838 mAh g^{-1} for MoO_2 and 1117 mAh g^{-1} for MoO_3) for LIBs.[7−9] Unfortunately, the phase transformation and large volume expansion occurred during the Li^+ insertion/extraction process, leading to breakdown of electrical pathways and detachment of the active material from the current collector and thereafter rapid capacity fading. To improve the cycling performance of MoO_2 electrode, many approaches have been considered including the formation of nanostructure and fabricating MoO_2−carbon composite. Nanostructured MoO_2 including nanofibers, nanospheres, and carbon hybrid nanocomposites have been demonstrated for high energy density with largely improved durability.[10−17] Mesoporous MoO_2 has also been used as an anode and exhibited a capacity of 750 mAh g^{-1} after 20 cycles at 35 mA g^{-1}.[10] Carbon-coated MoO_2 nanofiber showed a good cycling performance and delivered a capacity of 431 mA h g^{-1} after 50 cycles at 200 mA g^{-1}.[11] The anode made of carbon-coated MoO_2 nanocrystal delivered a reversible capacity of 629 mAh g^{-1} over 50 cycles at 200 mA g^{-1}.[13] MoO_2−carbon hybrid nanowires maintained a capacity of 327 mAh g^{-1} after 20 cycles at 1 A g^{-1}.[14] Ordered mesostructural carbon/metallic MoO_2 exhibited a fading capacity of 680 mA h g^{-1} after 20 cycles at 83 mA g^{-1}.[15] However, the reports dealing with MoO_2-based anode for high rate performance are still quite limited.

Recently, the carbon thermal reduction method was developed and considered as a rational and large-scalable synthetic route for fabricating low valence state materials.[18,19] On the other hand, the ordered mesoporous carbon (OMC) has been used as a promising carbon matrix for fabricating nanostructural electrode and exhibited a high Li-ion storage capability.[20,21]

In the present work, a carbon thermal reduction route was first applied to synthesize MoO_2−OMC nanocomposite using mesoporous carbon as the nanoreactor and reduction agent, and the synthesized nanocomposite exhibited large reversible capacity, high rate performance, and good cycling stability for Li-ion intercalation. Furthermore, the relationship between the

Received: December 29, 2012
Accepted: February 25, 2013
Published: February 25, 2013

   dx.doi.org/10.1021/am303286n | ACS Appl. Mater. Interfaces 2013, 5, 2182−2187

intrinsic characteristics of MoO_2−OMC nanocomposite and electrochemical properties was also discussed in detail.

EXPERIMENTAL SECTION

Preparation and Characterizations. The ordered mesoporous carbon (OMC) was used as a nanoreactor, and the phosphomolybdic acid (PMA) was the molybdenum resource. The synthetic process of OMC was similar to the report.[22] For a typical synthesis of MoO_2−C nanocomposite, OMC powders were dispersed in the concentrated HNO_3 (10 mL) and stirred for 1 h at 70 °C to induce hydrophilicity. Then, 1.58 g of PMA was dispersed in 10 mL of alcohol, and then, 0.1 g of OMC powder was added to the solution. After the ultrasonication for 30 min, the mixture was vigorous stirred overnight. The obtained mixture was heated at 75 °C for 2 h and then ground and calcined at 600 °C in Ar for 5 h. As a reference sample, bulk MoO_2 was also synthesized except for calcining at 600 °C in 5% H_2/95% Ar without OMC template.

X-ray diffraction (XRD) patterns were recorded on a PANalytical X'Pert spectrometer using the Co Kα radiation (λ = 1.789 Å), and the data would be changed to Cu Kα data. Scanning electron microscopy (SEM) and transmission electron microscopy (TEM) measurements were taken on a Hitachi 4800 instrument and a FEI F20 S-TWIN instrument, respectively. N_2 adsorption−desorption analysis was measured on a Micromeritics ASAP 2020 instrument; pore volumes were determined using the adsorbed volume at a relative pressure of 0.99. Multipoint Brunauer−Emmet−Teller (BET) surface area was estimated from the relative pressure range from 0.06 to 0.3. To determine the actual amount of carbon in the nanocomposites, thermogravimetric analysis (TGA) was performed using a CHNS/O analyzer (PE 2400II, Perkin-Elmer, America) in air atmosphere.

Electrochemical Measurements. For the electrochemical measurement, 80 wt % active materials (MoO_2−OMC nanocomposite) were mixed and grounded with 10 wt % polyvinylidene fluoride (PVDF) powder as a binder and 10 wt % acetylene black carbon (AB) powder as the conductive assistant materials. The mixture was spread and pressed on Cu foil circular flakes as the working electrode (WE) and dried at 120 °C for 12 h under the vacuum conditions. Metallic lithium foils were used as the negative electrodes. The electrolyte was 1 M $LiPF_6$ in a 1/1/1 (volume ratio) mixture of ethylene carbonate (EC), ethylene methyl carbonate (EMC), and dimethyl carbonate (DMC). The separator was UP 3093 (Japan) microporous polypropylene membrane. The electrochemical performance of OMC and bulk MoO_2 were also tested under the same conditions. The specific capacity values of MoO_2−OMC nanocomposite are calculated on the basis of the total mass of MoO_2 and OMC. Without any specific explanation, the galvanostatic charge and discharge experiment was performed in the range of 0.02−3.0 V at room temperature. The cells were assembled in a glovebox filled with highly pure argon gas (O_2 and H_2O levels <1 ppm), and charge/discharge tests were performed on a Land automatic batteries tester (Land CT 2001A, Wuhan, China). Electrochemical impedance spectroscopy (EIS) was performed on an IM6 electrochemical workstation.

RESULTS AND DISCUSSION

Figure 1 shows the XRD patterns of OMC, MoO_2−OMC nanocomposite, and bulk MoO_2. As seen from Figure 1a, two broad diffraction peaks at ca. 2θ of 22° and 43° were observed, which correspond to the (002) and (101) diffractions of graphite, suggesting the semigraphitized characterization of OMC. In Figure 1b, all diffraction peaks can be ascribed to the characteristic peaks of monoclinic MoO_2 (JCPDS 032-0671), confirming that MoO_2−OMC nanocomposite can be obtained. A mathematical analysis of the Bragg peaks was undertaken to calculate the crystallite size of MoO_2 in MoO_2−OMC nanocomposite using the Scherrer formula, and the particle size was found to be ca. 6.7 nm.

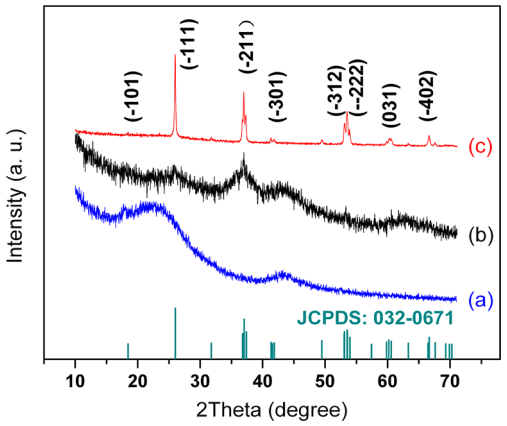

Figure 1. XRD patterns of (a) OMC, (b) MoO_2−OMC nanocomposite, and (c) bulk MoO_2, and standard XRD pattern of MoO_2.

SEM and TEM images of OMC and MoO_2−OMC nanocomposite are depicted in Figure 2. The ordered

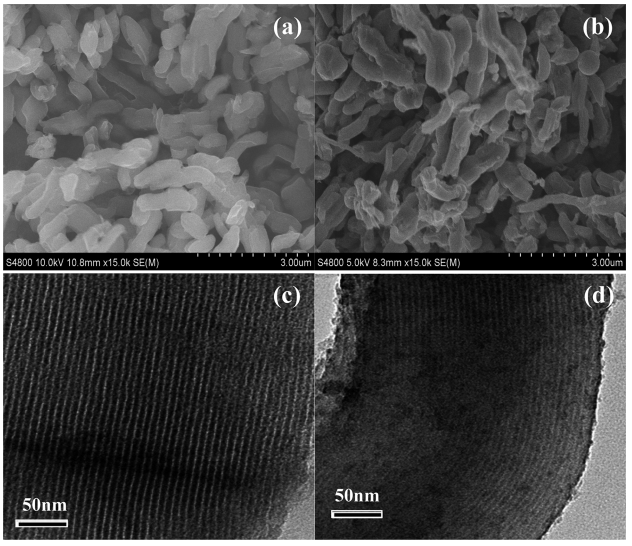

Figure 2. SEM and TEM images of (a, c) OMC and (b, d) MoO_2−OMC nanocomposite.

mesoporous carbon aggregates consisting of micrometer-sized rod-like particles were observed, as depicted in Figure 2a. The SEM image of MoO_2−OMC nanocomposite is depicted in Figure 2b, and the particle was not observed. Figure 2c shows the TEM image of OMC viewed along the direction of hexagonal pore arrangement, exhibiting the well ordered hexagonal arrangement of cylindrical mesoporous channels. It can be seen from Figure 2d that the mesoporous structure can remain very well for the MoO_2−OMC nanocomposite, and some MoO_2 nanoparticles are homogeneously incorporated into the channels of the ordered mesoporous carbon matrix. It was also confirmed that the size of MoO_2 nanoparticles in the MoO_2−OMC nanocomposite ranged from 4 to 10 nm, which was in agreement with the result of XRD measurement.

N_2 adsorption−desorption isotherms of OMC and MoO_2−OMC nanocomposite are depicted in Figure 3. BET surface area and pore volume were 1159 $m^2\ g^{-1}$ and 1.3 $cm^3\ g^{-1}$ for OMC and 407 $m^2\ g^{-1}$ and 0.32 $cm^3\ g^{-1}$ for MoO_2−OMC nanocomposite, respectively. This indicates that BET surface area and pore volume of MoO_2−OMC nanocomposite

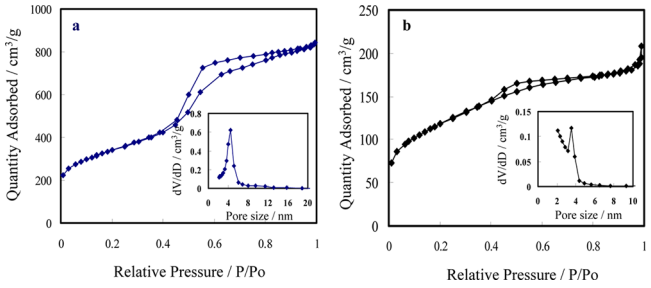

Figure 3. N_2 adsorption−desorption isotherms of (a) OMC and (b) MoO_2−OMC nanocomposite. Inset: Pore size distributions from the adsorption branch through the BJH method.

decreased significantly after incorporation of MoO_2 nanoparticle in the channels of OMC.

For quantifying the amount of carbon in the MoO_2−OMC nanocomposite, TGA was carried out in air and the result is depicted in Figure 4. The samples were heated from 50 to 680

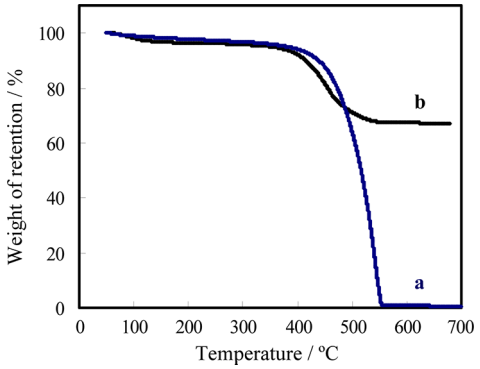

Figure 4. TGA curves of (a) OMC and (b) MoO_2−OMC nanocomposite.

°C at a rate of 5 °C min^{-1}. The weight loss below 150 °C was probably due to the evaporation of adsorbed moisture, considering the relatively high surface area of the samples. As can be seen from Figure 4a, the maximum weight loss of OMC took place at 400−550 °C. The weight change between 150 and 650 °C was due to both the oxidation of MoO_2 and the combustion of OMC. The theoretical value of the weight increase from MoO_2 to MoO_3 is 12.5 wt%. According to Figure 4b, it was estimated that the content of carbon was ca. 37 wt% for the MoO_2−OMC nanocomposite.

Figure 5 depicts the cycling performance of MoO_2−OMC nanocomposite operated at 50 mA g^{-1} for a potential window of 0.02−3 V. The capacity value was calculated on the total mass of MoO_2 and OMC. This material exhibited an initial discharge capacity of 1278 mA h g^{-1} and the charge capacity of 784 mA h g^{-1}, corresponding to a Coulombic efficiency of 61.4%. The initial irreversible capacity loss may be mainly attributed to irreversible processes such as inevitable formation of solid electrolyte interface (SEI layer) and electrolyte decomposition, which are common for most anode materials.[23] As can be seen, the capacity of MoO_2−OMC nanocomposite electrode decreased slightly after the initial 4 cycles and then remained stable after 50 cycles, meaning that the electrode has a good electrochemical stability and a high degree of reversibility. Importantly, the Coulombic efficiency becomes stable and is over 97% after the third cycle. A reversible capacity of 689 mA h g^{-1}, based on the mass of both MoO_2 and OMC,

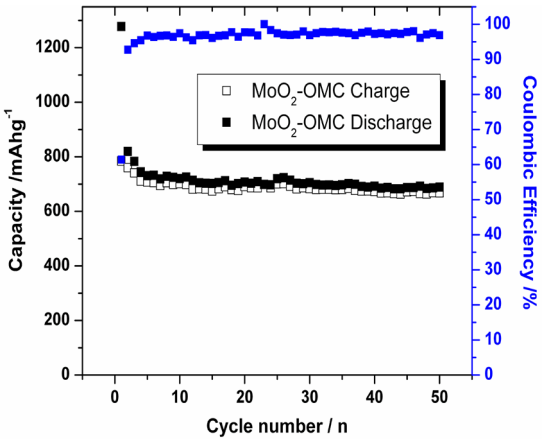

Figure 5. Cycling performance and Coulombic efficiency of MoO_2−OMC nanocomposite at a current density of 0.05 A g^{-1}.

can be achieved at a current density of 50 mA g^{-1} after 50 cycles, indicating the high performance of the MoO_2−OMC nanocomposite.

The electrochemical behaviors of the MoO_2−OMC nanocomposite electrodes were characterized by CV measurement at a scanning rate of 0.2 mV s^{-1} between 0.02 and 3.0 V, as shown in Figure 6a. In the first cycle, two reduction/oxidation pairs were observed at ca. 1.24/1.51 and 1.53/1.78 V, respectively, corresponding to the reversible phase transitions of partially lithiated Li_xMoO_2 during lithium insertion and extraction.[7] The second and fifth CV curves remained steady, which was in agreement with the charge/discharge curve properties. Figure 6b displays the charge−discharge potential profiles of MoO_2−OMC nanocomposite for the 1st, 2nd, 10th, 20th, 30th, and 50th cycle at a current density of 50 mA g^{-1}. The discharge curve profiles of MoO_2−OMC nanocomposite between the 10th and 50th cycle were overlapped, indicating the highly reversible performance of MoO_2−OMC nanocomposite electrode. The Li^+ insertion/extraction into/out of MoO_2 can be written as the following eqs 1 and 2.

$$x\mathrm{Li}^+ + x\mathrm{e}^- + \mathrm{MoO_2} \leftrightarrow \mathrm{Li}_x\mathrm{MoO_2} \quad (0 \le x \le 0.98) \quad (1)$$

$$\mathrm{Li}_{0.98}\mathrm{MoO_2} + 3.02\mathrm{Li} \leftrightarrow 2\mathrm{Li_2O} + \mathrm{Mo} \quad (2)$$

Figure 7 presents the cycling performance of MoO_2−OMC nanocomposite, OMC, and bulk MoO_2 at a current density of 0.1 A g^{-1} with a potential window of 3.0−0.02 V. The initial discharge capacities were 1901 and 543 mA h g^{-1} for OMC and bulk MoO_2 and then decreased to 404 and 73 mAh g^{-1} after 50 cycles, respectively. On the contrary, the anode made of MoO_2−OMC nanocomposite exhibited the discharge capacities of 781, 695, 680, and 668 mA h g^{-1} for the 2nd, 5th, 10th, and 50th cycle, respectively. As depicted in Figure 7, a capacity of 668 mA h g^{-1} can remain after 50 cycles at 0.1 A g^{-1} and was larger than that of MoO_2-based anodes in the previous reports.[24,25] Obviously, the capacity retention and cycling performance of the MoO_2−OMC nanocomposite was significant prior to those of OMC and bulk MoO_2, indicating that the mesoporous carbon support within MoO_2−OMC nanocomposite is beneficial to improve the electrochemical performance of MoO_2 anode.

Figure 8 presents the rate capability of MoO_2−OMC nanocomposite, OMC, and bulk MoO_2 at different current densities. The MoO_2−OMC nanocomposite kept a higher

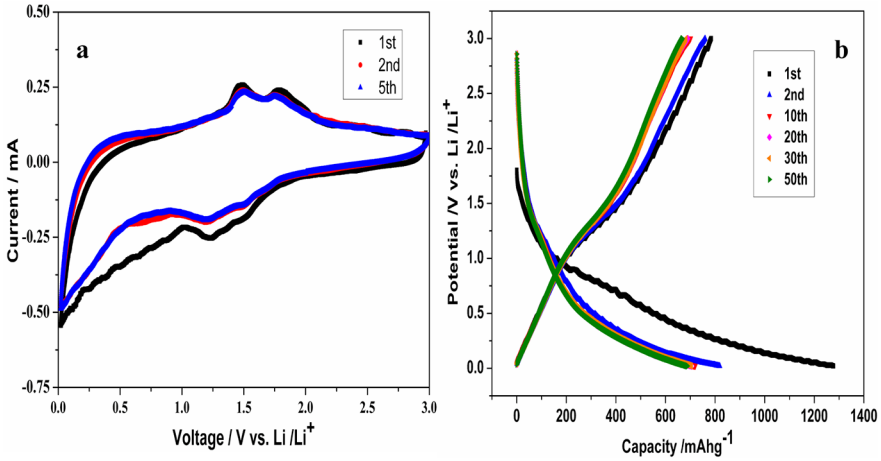

Figure 6. (a) Cyclic voltammograms of MoO_2−OMC nanocomposite at a scan rate of 0.2 mV s^{-1} between 0.02 and 3.0 V. (b) Charge and discharge profiles of MoO_2−OMC nanocomposite at a current density of 0.05 A g^{-1}.

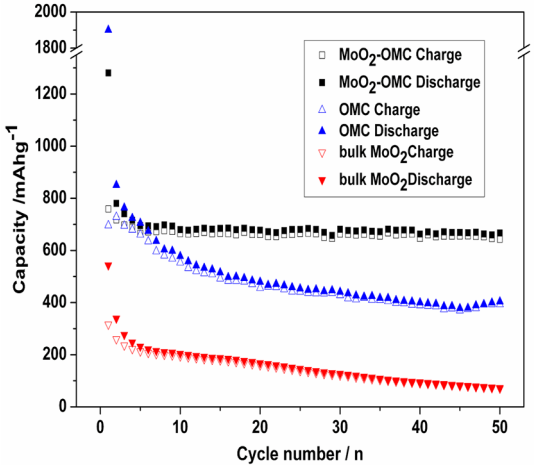

Figure 7. Cycling performance of MoO_2−OMC nanocomposite, OMC, and bulk MoO_2 at a current density of 0.1 A g^{-1}.

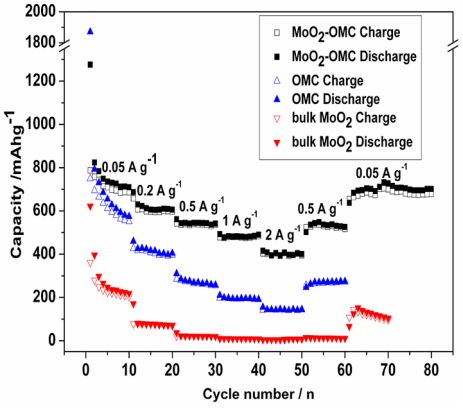

Figure 8. Rate capability of MoO_2−OMC nanocomposite, OMC, and bulk MoO_2 at different current densities.

reversible capacity after the 10th cycle at a current density of 0.05 A g^{-1}, while the reversible capacity for OMC and bulk MoO_2 anode dropped rapidly, which was basically in agreement with the previous reports.[10,21,25] The following reversible capacities of MoO_2−OMC nanocomposite were 606, 541, and 490 mA h g^{-1} at the current densities of 0.2, 0.5, and 1 A g^{-1}, respectively. Moreover, it is noteworthy that MoO_2−OMC nanocomposite has a stable capacity of 401 mA h g^{-1} even at a current density as high as 2 A g^{-1}, which was much larger than that of the previous reports,[10,14] indicating that the MoO_2−OMC nanocomposite delivered a high-rate performance. In addition, the capacity can be restored to its original state even if the current density returned to 0.05 A g^{-1} after 60 cycles. However, for the bulk MoO_2, the capacity decreased from 218 to 72, 20, 9, and 8 mA h g^{-1} when the charge/discharge current density was increased from 0.05 to 0.2, 0.5, 1, and 2 A g^{-1}, respectively. In a word, the rate capability of the MoO_2−OMC nanocomposite is prior to that of OMC and bulk MoO_2 anodes under the same conditions.

Figure 9 shows the Nyquist profiles of MoO_2−OMC nanocomposite, bulk MoO_2, and OMC. These data were

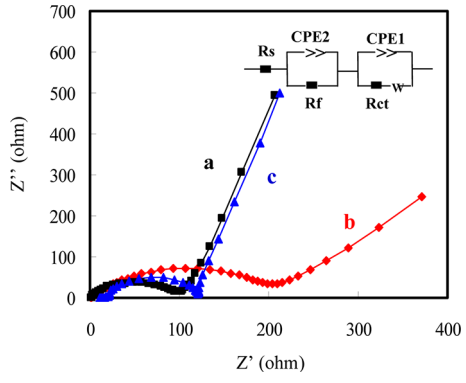

Figure 9. Impedance plots of (a) MoO_2−OMC nanocomposite, (b) bulk MoO_2, and (c) OMC. Inset: the equivalent circuit used to fit the experimental data.

collected after the 50th discharge−charge cycle. The simplified equivalent circuit in the inset of Figure 9 was used to interpret the measured results.[26] It can be seen that these plots are all composed of a semicircle at high frequencies which is related to the ohmic resistance and charge transfer resistance and a short inclined line in low frequency regions which is due to the ion diffusion within the anode. The semicircle for MoO_2−OMC nanocomposite was much smaller than that of bulk MoO_2, indicating that the mesoporous carbon can facilitate electron

transfer from embedded MoO_2 nanoparticles within the whole electrode and thus decrease resistance.

Table 1 lists the parameters of the equivalent circuit for MoO_2−OMC nanocomposite, bulk MoO_2, and OMC after fitting the diameter of the semicircular curve. Obviously, R_{ct} of MoO_2−OMC nanocomposite was much smaller than that of bulk MoO_2, suggesting that the electron transference of the former is prior to that of the latter.

Table 1. Impedance Parameters Calculated from an Equivalent Circuit Model

samples	R_s	R_f	R_{ct}
MoO_2−OMC	4	24	61
bulk MoO_2	5	35	157
OMC	11	29	62

The large capacity, excellent cyclic stability, and high rate performance of MoO_2−OMC nanocomposite might be ascribed to its unique structure and characterization, which favors both the electron transportation and electrolyte penetration. First, the high pore volume and open pore system with interconnected ordered mesopores would be favorable for the accessibility of the electrolyte, which makes the Li insertion/extraction more efficient, and restored more Li ion. Second, the homogeneously distributed MoO_2 nanoparticles of about 4−10 nm within the OMC channel offered a better accommodation of the strain and volume changes during the charge−discharge process, leading to highly cycling stability. Finally, the MoO_2−OMC nanocomposite with a large effective surface area and low charge transfer resistance could provide more sites for Li-ion insertion and a shorter path for Li-ion and electron transport, leading to the improved capacity and high rate capability.

CONCLUSIONS

In summary, the MoO_2−OMC nanocomposite was synthesized for the first time using a carbon thermal reduction route and the mesoporous carbon as the nanoreactor. It was found that the size of MoO_2 nanoparticles in the MoO_2−OMC nanocomposite ranged from 4 to 10 nm. The obtained MoO_2−OMC nanocomposite electrode exhibited large reversible capacity, high rate performance, and excellent long-term cycling stability. For instance, a high reversible capacity of 689 mA h g^{-1} can remain after 50 cycles at a current density of 50 mA g^{-1}. It is worth mentioning that the MoO_2−OMC nanocomposite electrode can attain a high reversible capacity of 401 mA h g^{-1} at a current density as high as 2 A g^{-1}. These results might be due to the fact that the MoO_2−OMC nanocomposite with a unique structure could provide more sites for Li-ion insertion and a shorter path for Li-ion and electron transport, leading to the improved capacity and excellent high rate performance. Thus, such MoO_2−OMC nanocomposite is a good candidate as anode material for high rate performance rechargeable LIBs. This facile strategy may be extended to fabricate other low valence state metal oxide−mesoporous carbon nanocomposites.

AUTHOR INFORMATION

Corresponding Author

*E-mail: wei-mingdeng@fzu.edu.cn. Tel/Fax: 86 591 83753180.

Notes

The authors declare no competing financial interest.

ACKNOWLEDGMENTS

This work was financially supported by National Natural Science Foundation of China (NSFC 21173049), National Science Foundation for Fostering Talents in Basic Research of National Natural Science Foundation of China (NSFC J1103303), and Key Laboratory of Novel Thin Film Solar Cells, CAS.

REFERENCES

(1) Dong, A.; Chen, J.; Vora, P. M.; Kikkawa, J. M.; Murray, C. B. *Nature* **2010**, *466*, 474−477.
(2) Srivastava, S.; Santos, A.; Critchley, K.; Kim, K. S.; Podsiadlo, P.; Sun, K.; Lee, J.; Xu, C.; Lilly, G. D.; Glotzer, S. C.; Kotov, N. A. *Science* **2010**, *327*, 1355−1359.
(3) Magasinki, A.; Dixon, P.; Hertzberg, B.; Kvit, A.; Ayala, J.; Yushin, G. *Nat. Mater.* **2010**, *9*, 353−358.
(4) Jia, H. P.; Gao, P. F.; Yang, J.; Wang, J. L.; Nuli, Y. N.; Yang, Z. *Adv. Energy Mater.* **2011**, *1*, 1036−1039.
(5) Zhao, Y.; Liu, X. Z.; Li, H. Q.; Zhai, T. Y.; Zhou, H. S. *Chem. Commun.* **2012**, *48*, 5079−5081.
(6) Wang, Y. G.; Li, H. Q.; He, P.; Hosono, E.; Zhou, H. S. *Nanoscale* **2010**, *2*, 1294−1305.
(7) Auborn, J. J.; Barberio, Y. L. *J. Electrochem. Soc.* **1987**, *134*, 638−641.
(8) (a) Yang, L. C.; Gao, Q. S.; Zhang, Y. H.; Tang, Y.; Wu, Y. P. *Electrochem. Commun.* **2008**, *10*, 118−122. (b) Sun, Y. M.; Hu, X. L.; Yu, J. C.; Li, Q.; Luo, W.; Yuan, L. X.; Zhang, W. X.; Huang, Y. H. *Energy Environ. Sci.* **2011**, *4*, 2870−2877.
(9) (a) Wang, Z. Y.; Madhavi, S.; Lou, X. W. *J. Phys. Chem. C* **2012**, *116*, 12508−12513. (b) Chen, J. S.; Cheah, Y. L.; Madhavi, S.; Lou, X. W. *J. Phys. Chem. C* **2010**, *114*, 8675−8678. (c) Fang, X. P.; Guo, B. K.; Shi, Y. F.; Li, B.; Hua, C. X.; Yao, C. H.; Zhang, Y. C.; Hu, Y. S.; Wang, Z. X.; Stucky, G. D.; Chen, L. Q. *Nanoscale* **2012**, *4*, 1541−1544.
(10) Shi, Y. F.; Guo, B. K.; Corr, S. A.; Shi, Q. H.; Heier, Y. S.; Hu, K. R.; Chen, L. Q.; Seshadri, R.; Stucky, G. D. *Nano Lett.* **2009**, *9*, 4215−4220.
(11) Luo, W.; Hu, X. L.; Sun, Y. M.; Huang, Y. H. *Phys. Chem. Chem. Phys.* **2011**, *13*, 16735−16740.
(12) Wang, Z. Y.; Chen, J. S.; Zhu, T.; Madhavi, S.; Lou, X. W. *Chem. Commun.* **2010**, *46*, 6906−6908.
(13) Zhou, L.; Wu, H. B.; Wang, Z. Y.; Lou, X. W. *ACS Appl. Mater. Interfaces* **2011**, *3*, 4853−4857.
(14) Gao, Q. S.; Yang, L. C.; Lu, X. C.; Mao, J. J.; Zhang, Y. H.; Wu, Y. P.; Tang, Y. *J. Mater. Chem.* **2010**, *20*, 2807−2812.
(15) Ji, X. L.; Herle, P. S.; Rho, Y.; Nazar, L. F. *Chem. Mater.* **2007**, *19*, 374−383.
(16) Sun, Y. M.; Hu, X. L.; Luo, W.; Huang, Y. H. *ACS Nano* **2011**, *5*, 7100−7107.
(17) Tang, Q. W.; Shan, Z. Q.; Wang, L.; Qin, X. *Electrochim. Acta* **2012**, *79*, 148−153.
(18) Saïdi, M. Y.; Barker, J.; Huang, H.; Swoyer, J. L; Adamson, G. *J. Power Source* **2003**, *119*−*121*, 266−272.
(19) Qiao, Y. Q.; Wang, X. L.; Zhou, Y.; Xiang, J. Y.; Zhang, D.; Shi, S. J.; Tu, J. P. *Electrochim. Acta* **2010**, *56*, 510−516.
(20) (a) Li, H. Q.; Zhou, H. S. *Chem. Commun.* **2012**, *48*, 1201−1217. (b) Wang, Y. G.; Wang, Y. R.; Hosono, E.; Wang, K. X.; Zhou, H. S. *Angew. Chem., Int. Ed.* **2008**, *47*, 7461−7465.
(21) (a) Ji, X. L.; Lee, K. T.; Nazar, L. F. *Nat. Mater.* **2009**, *8*, 500−506. (b) Zhou, H. S.; Zhu, S. M.; Hibino, M.; Honma, I.; Ichihara, M. *Adv. Mater.* **2003**, *15*, 2107−2111. (c) Wang, G. X.; Liu, H.; Liu, J.; Qiao, S. Z.; Lu, G. Q.; Munro, P.; Ahn, H. *Adv. Mater.* **2010**, *22*, 4944−4948. (d) Shen, L. F.; Zhang, X. G.; Uchaker, E.; Yuan, C. Z.; Cao, G. Z. *Adv. Energy Mater.* **2012**, *2*, 691−698. (e) Zeng, L. X.; Xiao, F. Y.; Wang, J. C.; Gao, S. K.; Ding, X. K.; Wei, M. D. *J. Mater. Chem.* **2012**, *22*, 14284−14288. (f) Zeng, L. X.; Zheng, C.; Xia, L. C.; Wang, Y. X.; Wei, M. D. *J. Mater. Chem. A* **2013**, DOI: 10.1039/C3TA10275K. (g) Chen, S. R.; Zhai, Y. P.; Xu, G. L.; Jiang, Y. X.;

Zhao, D. Y.; Li, J. T.; Huang, L.; Sun, S. G. *Electrochim. Acta* **2011**, *56*, 9549−9555.
(22) (a) Jun, S.; Joo, S. H.; Ryoo, R.; Kruk, M.; Jaroniec, M.; Liu, Z.; Ohsuna, T.; Terasaki, O. *J. Am. Chem. Soc.* **2000**, *122*, 10712−10713. (b) Zhao, D. Y.; Feng, J. L.; Huo, Q. S.; Melosh, N.; Fredrickson, G. H.; Chmelka, B. F.; Stucky, G. D. *Science* **1998**, *279*, 548−552. (c) Zeng, L. X.; Li, Q. F.; Chen, G. N.; Tang, D. P.; Wei, M. D. *Electrochim. Acta* **2012**, *68*, 158−165.
(23) Colbow, K. M.; Dahn, J. R.; Haering, R. R. *J. Power Sources* **1989**, *26*, 397−402.
(24) Yang, L. C.; Liu, L. L.; Zhu, Y. S.; Wang, X. J.; Wu, Y. P. *J. Mater. Chem.* **2012**, *22*, 13148−13152.
(25) Sun, Y. M.; Hu, X. L.; Luo, W.; Huang, Y. H. *J. Mater. Chem.* **2012**, *22*, 425−431.
(26) Cui, L. F.; Shen, J.; Cheng, F. Y.; Tao, Z. L.; Chen, J. *J. Power Sources* **2011**, *196*, 2195−2201.